

1 **Intraocular pressure, blood pressure and retinal blood flow autoregulation: a
2 mathematical model to clarify their relationship and clinical relevance**

3

4 Giovanna Guidoboni^{1,2*}, Alon Harris², Simone Cassani¹, Julia Arciero¹,
5 Brent Siesky², Annahita Amireskandari², Leslie Tobe², Patrick Egan², Ingrida
6 Januleviciene³, Joshua Park²

7

8 ¹Department of Mathematics, IUPUI, Indianapolis, IN 46202, USA.

9 ²Glick Eye Institute and Indiana University School of Medicine, Indianapolis, IN USA.

10 ³Eye Clinic, Lithuanian University of Health Sciences, Kaunas, Lithuania.

11

12 *Corresponding author. *E-mail address:* gguidobo@math.iupui.edu (G. Guidoboni).

13

14 **Abstract**

15 **Purpose:** This study investigates the relationship between intraocular pressure
16 (IOP) and retinal hemodynamics and predicts how arterial blood pressure (BP) and
17 blood flow autoregulation (AR) influence this relationship.

18 **Methods:** A mathematical model is developed to simulate blood flow in the
19 central retinal vessels and retinal microvasculature as current flowing through a network
20 of resistances and capacitances. Variable resistances describe active and passive
21 diameter changes due to AR and IOP. The model is validated using clinically measured
22 values of retinal blood flow and velocity. The model simulations for six theoretical
23 patients with high, normal and low BP (HBP-, NBP-, LBP-) and functional or absent AR

24 (-wAR, -woAR) are compared with clinical data.

25 **Results:** The model predicts that NBPwAR and HBPwAR patients can regulate
26 retinal blood flow (RBF) as IOP varies between 15 and 23 mmHg and between 23 and
27 29 mmHg, respectively, while LBPwAR patients do not adequately regulate blood flow if
28 IOP is 15 mmHg or higher. Hemodynamic alterations would be noticeable only if IOP
29 changes occur outside of the regulating range which, most importantly, depends on BP.
30 The model predictions are consistent with clinical data for IOP-reduction via surgery and
31 medications and for cases of induced IOP-elevation.

32 **Conclusions:** The theoretical model results suggest that the ability of IOP to
33 induce noticeable changes in retinal hemodynamics depends on the levels of BP and AR
34 of the individual. These predictions might help to explain the inconsistencies found in the
35 clinical literature concerning the relationship between IOP and retinal hemodynamics.

36 **Keywords:** intraocular pressure, retina, blood flow, mathematical model,
37 autoregulation

38

39 1 Introduction

40 Alterations in retinal and retrobulbar hemodynamics are associated with many
41 ocular and systemic diseases, including glaucoma¹⁻³, age-related macular
42 degeneration^{4, 5} and diabetes^{5, 6}. Since the retinal vasculature is in direct contact with the
43 intraocular pressure (IOP), it seems very likely that IOP has an impact on retinal blood
44 flow and velocity. However, clinical evidence of such an impact is not unanimous.
45 Several clinical studies showed a decrease in retinal and retrobulbar blood flow and
46 velocity when IOP was increased⁷⁻¹⁴, while other studies did not find any significant

47 changes in retinal and retrobulbar hemodynamics with changes in IOP¹⁵⁻²⁷.

48 Most of the hemodynamic measurements obtained after trabeculectomy provide
49 evidence of increased blood velocity as a result of lowering IOP^{9, 13, 14}. Galassi et al.⁹
50 found that, following trabeculectomy, end-diastolic velocity (EDV) was increased and
51 resistive index (RI) was decreased in the ophthalmic artery (OA), central retinal artery
52 (CRA), and short posterior ciliary arteries (SPCAs). Similarly, Trible et al.¹⁴ found
53 sustained increases in mean flow velocity (MFV) and EDV and decreases in RI in the
54 CRA and SPCAs after trabeculectomy. Synder et al.¹³ demonstrated an increase in
55 blood velocity in the posterior ciliary arteries (PCAs) in the 18 trabeculectomy cases they
56 investigated. However, Cantor¹⁷ found that despite a mean IOP reduction of 17.1 mmHg,
57 15.5 mmHg and 15.1 mmHg at 3, 6 and 12 months after trabeculectomy, respectively,
58 the 17 glaucoma patients evaluated in the study did not show any significant change in
59 ocular hemodynamic parameters.

60 The effects of IOP-lowering topical medications (such as prostaglandin
61 analogues, carbonic anhydrase inhibitors, and beta blockers) on retrobulbar
62 hemodynamics have also been assessed. Some studies found slightly increased
63 retrobulbar circulation in patients on these medications^{7, 11, 12}, while most of the studies
64 found that treatment with topical medications did not have a significant effect on
65 retrobulbar hemodynamics^{15, 16, 19-23, 25-27}.

66 Only a few studies have been conducted to evaluate the effect of IOP elevations
67 on ocular hemodynamics, and these have also provided variable results. Harris et al.¹⁰
68 used suction ophthalmodynamometry to increase IOP from a baseline average value of
69 14 mmHg to 45 mmHg in 11 healthy subjects. In the CRA, peak systolic velocity (PSV)

70 and EDV decreased and the RI increased in steady progression as IOP was acutely
71 elevated, while no changes occurred in the OA. Findl et al.⁸ found that increased IOP
72 (+10, +20 mmHg via suction cup) led to decreased blood velocities (as measured by
73 Doppler sonography) in the CRA in 10 healthy volunteers, but no changes in the OA.
74 However, Conway et al.¹⁸ used suction with laser in situ keratomileusis (IOP was
75 elevated above 85 mmHg for 90 seconds) in 10 healthy subjects and no hemodynamic
76 changes were found after releasing the suction (as measured by Color Doppler Imaging
77 (CDI), Heidelberg Retinal Flowmeter (HRF) and ocular blood-flow analyzer).

78 In summary, clinical evidence for the relationship between changes in IOP and
79 consequent changes in retinal and retrobulbar hemodynamics is inconsistent and
80 therefore difficult to interpret. However, the inconsistent results are likely due to the
81 numerous factors, including arterial blood pressure^{2, 28-32} and blood flow autoregulation²,
82 ³³⁻³⁵, that influence the relationship between IOP and ocular hemodynamics and the
83 intrinsic difficulty of evaluating the individual contribution of these factors in a clinical
84 setting.

85 Mathematical modeling can be used to investigate the complex relationship
86 between IOP and retinal and retrobulbar hemodynamics by assessing the mechanical
87 action of IOP on clinically-measurable hemodynamic quantities such as total retinal
88 blood flow and CRA blood velocity^{36, 37}. Over the last two decades, theoretical models
89 have been used to study stress and strain distributions induced by IOP elevation in
90 ocular tissues³⁸⁻⁵⁶, most importantly in the lamina cribrosa, although these models did
91 not consider blood supply to the tissue. Theoretical models have also been used to
92 assess the artero-venous distribution of hemodynamic parameters in the retinal

93 microvasculature⁵⁷⁻⁶⁰, but they did not consider the biomechanical response of the retinal
94 vasculature to IOP. Recently, Arciero et al.⁶¹ used a theoretical model to study the retinal
95 microcirculation and predict the relative importance of regulatory mechanisms in
96 achieving blood flow autoregulation, but the model did not incorporate the effects of the
97 hemodynamics in the central retinal vessels. Guidoboni et al.⁶² used a theoretical model
98 to study the effects of IOP elevation on CRA hemodynamics, but the model was not
99 linked to the blood circulation in the retinal microvasculature.

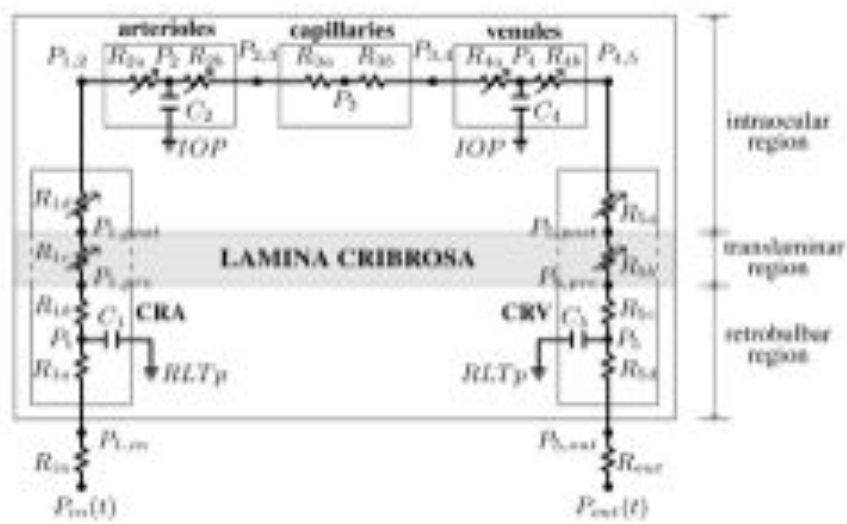
100 The current study introduces the first mathematical model that simultaneously
101 accounts for (i) blood flow in the central retinal vessels; (ii) blood flow in the retinal
102 microvasculature; (iii) retinal blood flow autoregulation; (iv) biomechanical action of IOP
103 on the retinal vasculature; and (v) time-dependent arterial blood pressure. The model
104 employs a hydraulic analogy to Ohm's law in which blood flow in the central retinal
105 vessels and retinal microvasculature is analogous to the current flowing through a
106 network of resistances and capacitances. Variable resistances describe active and
107 passive diameter changes due to blood flow autoregulation and IOP, and systemic
108 arterial blood pressure is an input to the model. Model outputs include total retinal blood
109 flow and blood velocity in the CRA, CRV and microvasculature, thereby allowing for
110 direct comparison between model predictions and clinically-measurable quantities. The
111 main goal of the present study is to use this mathematical model to interpret the
112 inconsistent clinical observations concerning the relationship between IOP and retinal
113 and retrobulbar hemodynamics.

114

115

116 **2 Methods**

117 The retinal vasculature is represented by the model depicted in Figure 1. The
118 vasculature is divided into five main compartments: the central retinal artery (CRA),
119 arterioles, capillaries, venules, and the central retinal vein (CRV). Using the analogy
120 between hydraulic and electrical circuits, blood flow is modeled as current flowing
121 through a network of resistors (R), representing the resistance to flow offered by blood
122 vessels, and capacitors (C), representing the ability of blood vessels to deform and store
123 blood volume. Resistors and capacitors have been labeled with numbers from 1 to 5 to
124 distinguish between compartments, and additional alphabetic labels are used to
125 distinguish between segments within the same compartment. For example, the CRA
126 compartment is referenced by the label 1 and it includes a retrobulbar segment with
127 resistances R_{1a} and R_{1b} , a translaminar segment with resistance R_{1c} and an intraocular
128 segment with resistance R_{1d} . We remark that the resistance of the retrobulbar segment
129 has been split into R_{1a} and R_{1b} so that the capacitance C_1 acts on the mean retrobulbar
130 pressure, P_1 . The blood flow through the retinal vascular network is driven by P_{in} and
131 P_{out} , which represent the blood pressures upstream of the CRA and downstream of the
132 CRV, respectively.



133

134 **Figure1:** Network model for the retinal vasculature. The vasculature is divided
 135 into five main compartments: the central retinal artery (CRA), arterioles, capillaries,
 136 venules, and the central retinal vein (CRV). Each compartment includes resistances (R)
 137 and capacitances (C). The intraocular segments are exposed to the intraocular pressure
 138 (IOP), the retrobulbar segments are exposed to the retrolaminar tissue pressure (RLTp),
 139 and the trans-laminar segments are exposed to an external pressure that depends on
 140 the internal state of stress within the lamina cribrosa (gray shaded area). Diameters of
 141 venules and intraocular and translaminar segments of the CRA and CRV are assumed to
 142 vary passively with IOP, while arterioles are assumed to be vasoactive.
 143

144 The vascular segments are exposed to various external pressures depending on
 145 their position in the network. The intraocular segments are exposed to the IOP, the
 146 retrobulbar segments are exposed to the retrolaminar tissue pressure (RLTp), and the
 147 trans-laminar segments are exposed to an external pressure that depends on the
 148 internal state of stress within the lamina cribrosa. The IOP-induced stress within the
 149 lamina cribrosa is computed using a nonlinear elastic model described in the Appendix.

150 The resistances of the venules and intraocular and translaminar segments of the
 151 CRA and CRV are assumed to vary passively with IOP, as detailed in the Appendix. The
 152 resistance of arterioles is assumed to vary actively to achieve a relatively constant blood
 153 flow despite changes in the ocular perfusion pressure (OPP), defined as OPP = 2/3 MAP

154 – IOP, where MAP is the mean arterial pressure at the level of the brachial artery (MAP =
 155 2/3 DP + 1/3 SP), and DP and SP are diastolic and systolic arterial blood pressures,
 156 respectively. Arrows have been used in Figure 1 to indicate all resistances that can vary,
 157 either passively or actively.

158 **Governing equations.** Ohm's law states that the flow Q through a resistor is
 159 directly proportional to the pressure drop ΔP across the resistor, with a proportionality
 160 constant equal to the reciprocal of the resistance, namely $Q = \Delta P/R$. The flow Q through
 161 a capacitor is directly proportional to the time derivative of the pressure drop across the
 162 capacitor, with a proportionality constant equal to the capacitance, namely $Q = C$
 163 $d(\Delta P)/dt$. Kirchoff's law guarantees the conservation of mass in the system, which
 164 means that at every network node the following relationship must hold: *volume change* =
 165 *flow in – flow out*. The application of Kirchoff's law to the retinal vascular network shown
 166 in Figure 1 leads to the following system of ordinary differential equations for the
 167 pressures (P):

$$\left\{ \begin{array}{l} C_1 \frac{d(P_1 - RLT_p)}{dt} = \frac{P_{in} - P_1}{R_{in} + R_{1a}} - \frac{P_1 - P_2}{R_{1b} + R_{1c} + R_{1d} + R_{2a}} \\ C_2 \frac{d(P_2 - IOP)}{dt} = \frac{P_1 - P_2}{R_{1b} + R_{1c} + R_{1d} + R_{2a}} - \frac{P_2 - P_4}{R_{2b} + R_{3a} + R_{3b} + R_{4a}} \\ C_4 \frac{d(P_4 - IOP)}{dt} = \frac{P_2 - P_4}{R_{2b} + R_{3a} + R_{3b} + R_{4a}} - \frac{P_4 - P_5}{R_{4b} + R_{5a} + R_{5b} + R_{5c}} \\ C_5 \frac{d(P_5 - RLT_p)}{dt} = \frac{P_4 - P_5}{R_{4b} + R_{5a} + R_{5b} + R_{5c}} - \frac{P_5 - P_{out}}{R_{5d} + R_{out}} \end{array} \right. . \quad (1)$$

168 The inlet and outlet pressures P_{in} and P_{out} vary with time along a cardiac cycle and,
 169 consequently, the pressures calculated via equations (1) are time dependent.

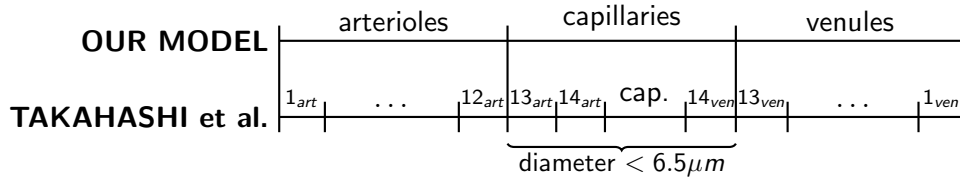
170 **Control values of flow rate, resistances, pressures and capacitances.** A
 171 control state for the system is defined to represent typical conditions of a healthy eye.
 172 Control values of any given quantity will be indicated with an overline bar.

173 *External and systemic pressures.* We assume that, for a healthy individual, \overline{IOP}
174 = 15 mmHg⁶³⁻⁶⁵, \overline{RLTp} = 7 mmHg^{66, 67}, \overline{SP} = 120 mmHg, and \overline{DP} = 80 mmHg.

175 *Retinal blood flow.* The control value \bar{Q} of the retinal blood flow can be estimated
176 by applying Poiseuille's law to the CRA, since the CRA is the only vessel supplying blood
177 to the retinal vascular network. In the hypotheses of laminar flow and cylindrical
178 geometry, Poiseuille's law yields $\bar{Q} = \pi \bar{V}_{cra,max} D_{cra}^2 / 8$, where D_{cra} is the CRA diameter,
179 and $\bar{V}_{cra,max}$ is the average value of the CRA centerline velocity over a cardiac cycle.
180 Measurements from human patients are used to define the control state values for $D_{cra} =$
181 175 μm ⁶⁸, and $\bar{V}_{cra} = 5.67 \text{ cm/s}$ ^{10, 68}, which yield a physiological value of $\bar{Q} = 6.8178 \cdot$
182 10^{-4} ml/s ⁶⁸⁻⁷².

183 *Resistances.* According to Poiseuille's law, the resistance of a vessel is
184 $R = 128\mu L/\pi D^4$, where D and L are vessel diameter and length and μ is the blood
185 viscosity. Using this law and the data reported in Table 1, the control values of the CRA
186 and CRV resistances are computed and summarized in Table 2. Determining the control
187 values of arteriolar, capillary and venular resistances is more complex, since these
188 compartments include a hierarchy of numerous vessels of various diameter. We adopt
189 the dichotomous network (DN) model for the retinal microcirculation proposed by
190 Takahashi et al.⁶⁰ to describe the hierarchical architecture of arterioles, capillaries and
191 venules and compute their resistances. The DN model includes 14 levels of arterioles, 1
192 level of capillaries and 14 levels of venules; each level includes a specific number of
193 parallel vessels. In our model framework, we divided these 29 vascular levels into the
194 corresponding model compartments according to vessel size. All the vessels with
195 diameter less than 6.5 μm were defined as capillaries, as shown in Figure 2. Vessel

196 number, diameter, length and blood viscosity for the 29 levels in the DN model are
 197 reported in reference⁶⁰, and the corresponding values of the lumped resistances used in
 198 the current model are summarized in Table 2. It is important to note that the viscosity
 199 values used in the model are effective viscosity values that are based on an empirical
 200 relationship and depend on vessel diameter. In this way, the model takes into account
 201 the corpuscular nature of blood. R_{in} and R_{out} incorporate the vasculature upstream of
 202 the CRA and downstream of the CRV. Their control values are determined by the control
 203 value \bar{Q} of the total retinal blood flow and the control values of pressures \bar{P}_{in} , $\bar{P}_{1,in}$, and
 204 \bar{P}_{out} , $\bar{P}_{5,out}$ (defined below).



205

206 **Figure 2:** Relationship between the dichotomous network (DN) model by
 207 Takahashi et al.⁶⁰ and the chosen geometry of our model. The 29 vascular levels of the
 208 DN model have been divided into three model compartments for arterioles, capillaries
 209 and venules according to vessel size.
 210

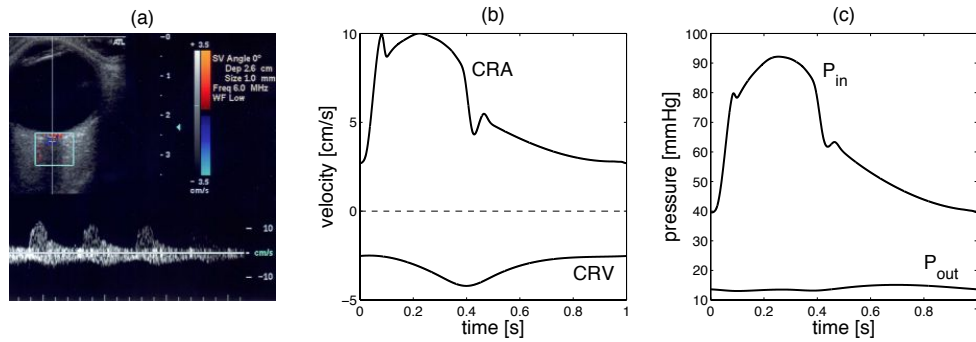
211 **Pressures.** The control value of the input pressure is chosen to be 2/3 of the mean
 212 arterial pressure (MAP) measured at the level of the brachial artery, where the factor 2/3
 213 accounts for the distance from the brachial artery to the eye⁷³. Since $\bar{SP} = 120$ mmHg
 214 and $\bar{DP} = 80$ mmHg, it follows that $\bar{P}_{in} = 62.2$ mmHg, as reported in Table 3. The
 215 control pressure between arterioles and capillaries, $\bar{P}_{2,3}$, is set at 32 mmHg^{61, 74}. The
 216 control pressures at all the other nodes of the network are computed using Ohm's law
 217 and the previously computed control values of the resistances, namely $\bar{P}_i = \bar{P}_j -$
 218 $\bar{R}_{i,j}\bar{Q}$, where the subscripts i and j indicate any two consecutive nodes and $\bar{R}_{i,j}$ the

219 resistance between them. The control value of the outlet pressure is chosen to be \bar{P}_{out}
220 = 14 mmHg so that it is less than $\bar{P}_{5,out}$ and higher than the jugular venous pressure
221 (normally between 4 and 6 mmHg⁷⁵). All control pressures are summarized in Table 3.

222 **Capacitances.** The capacitance of a fluid compartment represents its ability to
223 store fluid volume for a given difference between the pressure inside and outside the
224 compartment. The capacitance of vascular compartments can be computed as the
225 product of vascular volume (*Vol*) and distensibility (*Dist*)⁷⁶. The control values of the CRA
226 and CRV volumes are computed as $\overline{Vol}_{cra} = \pi D_{cra}^2 L_{cra}/4$ and $\overline{Vol}_{crv} = \pi D_{crv}^2 L_{crv}/4$.
227 Analogously, the control values of the volumes of arterioles, capillaries and venules are
228 computed using the level architecture and data reported by Takahashi et al.⁶⁰. The
229 distensibilities of the CRA and the retinal arterioles are assumed to be equal to those of
230 the cerebral arteries⁷⁶, namely $Dist_{cra} = Dist_2 = 34.12 \cdot 10^{-4}$ mmHg⁻¹. Following the
231 work by Lakin et al.⁷⁶, the distensibilities of retinal venules and the CRV are assumed to
232 be 8 times larger than those of the arteries, namely $Dist_{crv} = Dist_4 = 27.30 \cdot 10^{-3}$
233 mmHg⁻¹. The control volumes and capacitances are reported in Table 4.

234 **Time-profiles of the input and output pressure waves.** The time profile of P_{in}
235 and P_{out} at the control state are determined through an inverse problem based on CDI
236 measurements of blood velocity in the CRA and CRV, as shown in Figure 3(a). The
237 centerline blood velocity $V(t)$ in the CRA and CRV is given by $V(t) = 8 Q(t)/\pi D^2$, where
238 $Q(t) = \Delta P(t)/R(t)$ and $\Delta P(t)$ is the pressure drop across the resistor. Thus, equations
239 (1) can be used to determine the time-profiles $P_{in}(t)$ and $P_{out}(t)$ that give the CRA blood
240 velocity profiles shown in Figure 3(b) when the system is at its control state. The control
241 profiles of $\bar{P}_{in}(t)$ and $\bar{P}_{out}(t)$ are shown in Figure 3(c), and their mean values are

242 $\bar{P}_{in} = 62.2$ mmHg and $\bar{P}_{out} = 14$ mmHg. At the control state, the maximum and
 243 minimum values of $\bar{P}_{in}(t)$ are $\bar{P}_{in,max} = 92.2$ mmHg and $\bar{P}_{in,min} = 39.6$ mmHg, and
 244 their ratios with respect to \overline{SP} and \overline{DP} are $\bar{P}_{in,max}/\overline{SP} = 0.7683$ and $\bar{P}_{in,min}/\overline{DP} =$
 245 0.4945. These ratios are used to scale the $P_{in}(t)$ profile in the simulations of clinical
 246 conditions where SP and DP are different from their control state values.



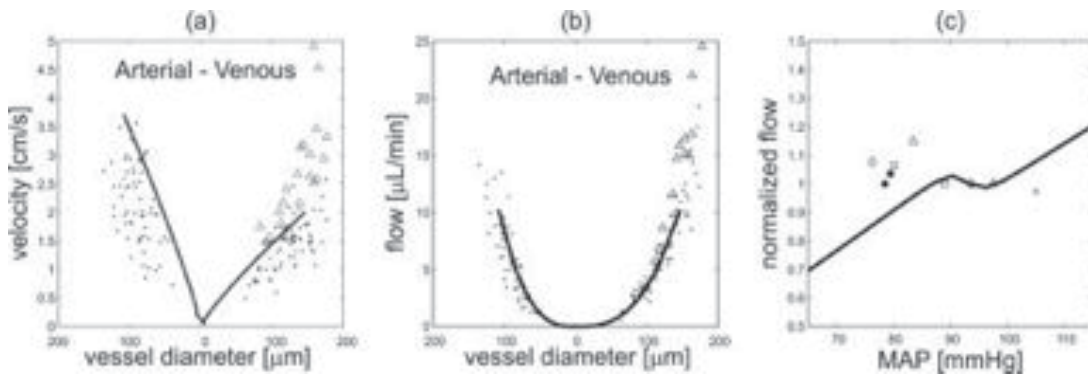
247
 248 **Figure 3** (a) Typical CDI measurement of the blood velocity in the CRA and CRV.
 249 (b) Time profiles of the blood velocity in the CRA and CRV at the control state. (c) Time
 250 profile of the inlet and outlet pressures $\bar{P}_{in}(t)$ and $\bar{P}_{out}(t)$ at the control state.
 251

252 **3 Results**

253 In this study, Matlab is used to solve equations (1) for six different cases
 254 corresponding to different clinical conditions. Specifically, the six cases represent
 255 patients with high, normal and low arterial blood pressure (HBP-, NBP-, LBP-), with
 256 functional or absent blood flow autoregulation (-wAR, -woAR), as summarized in Table
 257 5. Systolic/diastolic arterial blood pressures for cases HBP-, NBP- and LBP- are
 258 assumed to be 140/90 mmHg, 120/80 mmHg and 100/70 mmHg, respectively.
 259 Functional autoregulation is simulated by allowing arteriolar resistances R_{2a} and R_{2b} to
 260 vary according to equation (3) in the Appendix. To simulate the absence of

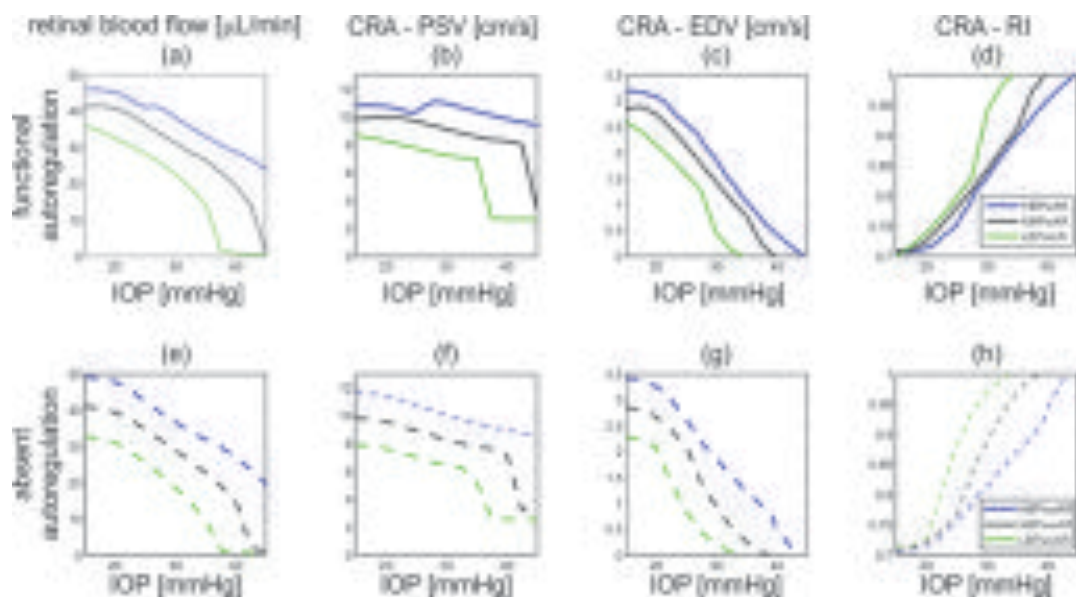
261 autoregulation, arteriolar resistances R_{2a} and R_{2b} do not change and are set equal to
262 their control values \bar{R}_{2a} and \bar{R}_{2b} .

263 **Model validation.** The model predicted mean values of blood velocity and flow
264 along the retinal vascular network obtained for the NBPwAR case, representing a normal
265 clinical condition, are compared in Figures 4(a) and 4(b) with measurements obtained by
266 Garcia et al.⁷⁷ and Riva et al.⁷⁸ using bidirectional laser Doppler velocimetry in healthy
267 individuals. The pressures at each node of the network are computed from equations (1)
268 and then velocity and flow in arterioles, capillaries and venules are determined assuming
269 the network architecture proposed by Takahashi et al.⁶⁰. The model predicted values of
270 total retinal blood flow for IOP = 15 mmHg and MAP between 65 and 115 mmHg are
271 compared with data measured by Dumskyj et al.⁶⁹, Feke and Pasquale⁷⁰, Feke et al.⁷¹
272 and Harris et al.⁶³ in Figure 4(c). The model predicted values are normalized with respect
273 to the control state, and the measured data are normalized with respect to their reported
274 baseline value.



275
276 **Figure 4:** (a) Comparison of model predicted values (*solid line*) of blood velocity with
277 measured data (*open triangles*⁷⁷, *black dots*⁷⁸) for vessels of various diameter. (b)
278 Comparison of model predicted values (*solid line*) of volumetric blood flow with
279 measured data (*open triangles*⁷⁷, *black dots*⁷⁸) for vessels of various diameter. (c)
280 Comparison of model values (*solid line*) of normalized total retinal blood flow with
281 measured data (*black dots*⁶⁹, *open triangles*⁷⁰, *open squares*⁷⁰, *open diamonds*⁷¹,
282 *pluses*⁶³) for various mean arterial pressures (MAP). In all model simulations IOP = 15
283 mmHg.

284 **Theoretical investigations.** The mathematical model is used to investigate the
 285 effects of blood pressure and blood flow autoregulation on the IOP-induced
 286 hemodynamic changes in total retinal blood flow, CRA blood velocity and intraluminal
 287 blood pressure along the retinal vasculature. The model predictions for total retinal blood
 288 flow, computed as the time-average of $Q(t)$ over a cardiac cycle, PSV, EDV and RI in the
 289 CRA are compared for cases NBPwAR, NBPwoAR, HBPwAR, HBPwoAR, LBPwAR and
 290 LBPwoAR in Figure 5.



297 **Figure 5:** Model predicted values of total retinal blood flow; peak systolic velocity
 298 in the central retinal artery (CRA - PSV); end diastolic velocity in the CRA (CRA – EDV);
 299 and resistivity index in the CRA (CRA-RI) as IOP varies between 15 and 40 mmHg for
 300 theoretical patients with low, normal or high blood pressure (LBP-, NBP-, HBP-) and
 301 functional or absent blood flow regulation (-wAR, -woAR).

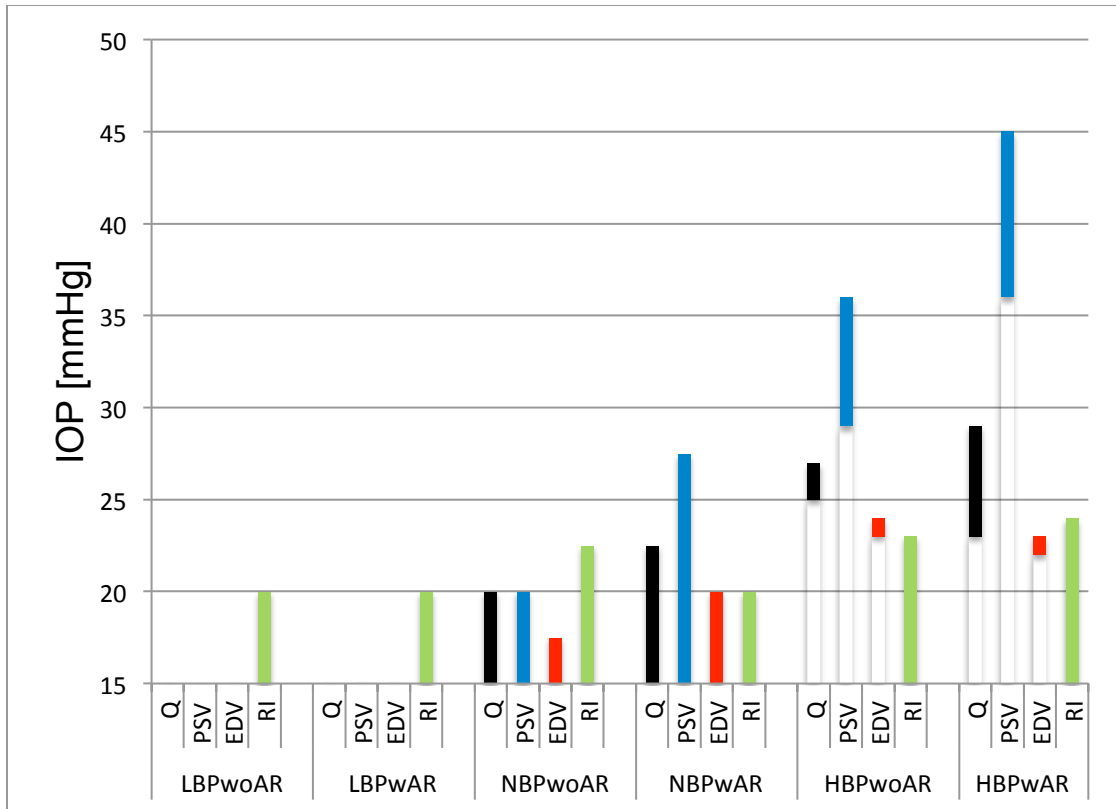
303 Figure 6 reports the IOP ranges for which the values of total retinal blood flow (Q),
 304 and PSV, EDV and RI in the CRA are within $\pm 5\%$ of their control values, as predicted by
 305 the mathematical model for six theoretical patients. In the low blood pressure cases
 306 (LBPwAR and LBwoAR), the values of Q , PSV and EDV are never within 5% of their

307 control values. The small (5%) change in blood flow is chosen as a rough threshold for
308 quantifying the regime when autoregulation is successful.

309 *Total retinal blood flow.* As shown in Figures 5 and 6, the model predicted
310 average blood flow over a cardiac cycle remains relatively constant for IOP between 15
311 and 23 mmHg for NBPwAR individuals. In the HBPwAR case, relatively constant flow is
312 predicted for IOP between 23 and 29 mmHg. In the remaining cases, the model predicts
313 a slight or nonexistent autoregulation plateau for IOP between 15 to 45 mmHg.

314 *CRA blood velocity.* Although a monotone decrease in PSV and EDV with IOP
315 elevation is predicted in most of the theoretical patients, Figures 5(b) and 5(c) show that
316 the NBPwAR and HBPwAR cases exhibit a slight PSV increase for IOP within the
317 regulating range, namely between 15 and 23 mmHg for NBPwAR and between 23 and
318 29 mmHg for HBPwAR. For all six cases, the model predicts an increase of the CRA
319 resistivity index $RI = (PSV-EDV)/PSV$ with IOP, as shown in Figures 5(d) and 5(h). As
320 shown in Figure 6, the range of IOP for which PSV is within 5% of its control values is
321 significantly larger than the range for EDV, and the ranges do not overlap in the
322 HBPwAR and HBPwoAR cases.

323

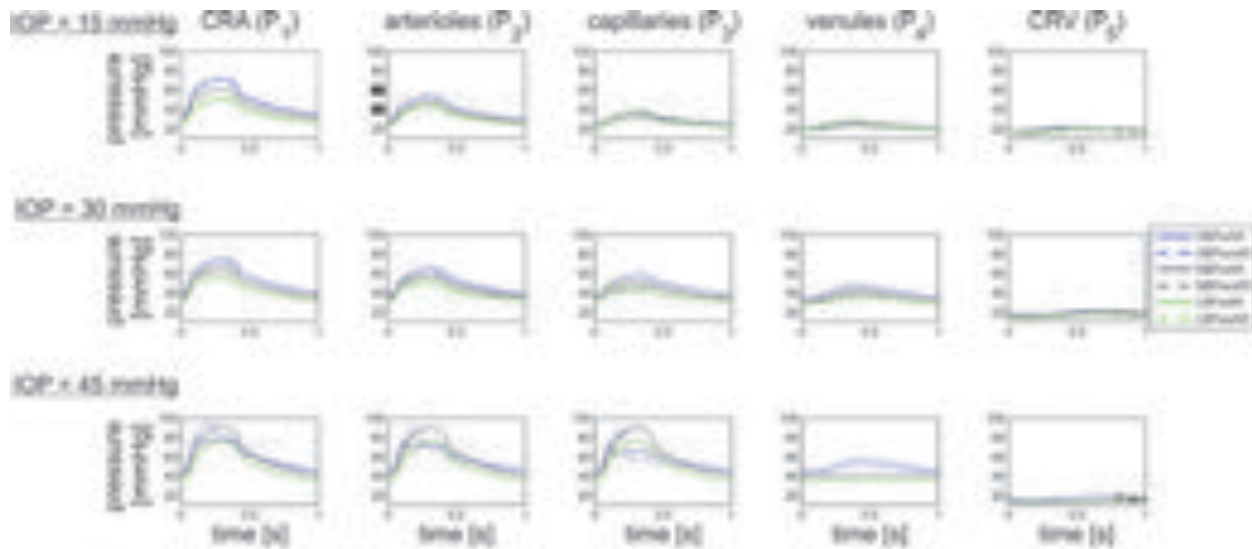


324

325 **Figure 6.** Model predicted ranges of IOP for which the values of total retinal
 326 blood flow (Q, black), PSV (blue), EDV (red) and RI (green) are within $\pm 5\%$ of their
 327 control state values for six theoretical patients with low, normal or high blood pressure
 328 (LBP-, NBP-, HBP-) and functional or absent blood flow regulation (-wAR, -woAR).

329

330 *Intraluminal blood pressure.* The model predicted values of blood pressure in the
 331 five model compartments of the retinal vasculature for IOP equal to 15, 30 and 45 mmHg
 332 are compared in Figure 7 for the six representative clinical cases described in Table 5.
 333 Pronounced changes in pressure are visible in the CRA, arterioles, capillaries and
 334 venules with IOP elevation, while the pressure in the CRV remains relatively constant.
 335 As expected, when IOP is sufficiently high, the venules collapse. The degree to which
 336 the vessels collapse depends on the MAP of the individual. In particular, the model
 337 predicts that for an IOP = 45 mmHg, the venules are collapsed to a lesser extent in HBP-
 338 patients than in NBP- and LBP- patients.



339

340 **Figure 7:** Model predicted values of blood pressure in CRA (P_1),
 341 arterioles (P_2), capillaries (P_3), venules (P_4), and CRV (P_5) for IOP = 15, 30,
 342 and 45 mmHg for six theoretical patients with high (blue), normal (black)
 343 and low (green) blood pressure (HBP-, NBP-, LBP-), and functional (solid)
 344 or absent (dashed) blood flow regulation (-wAR, -woAR).

345

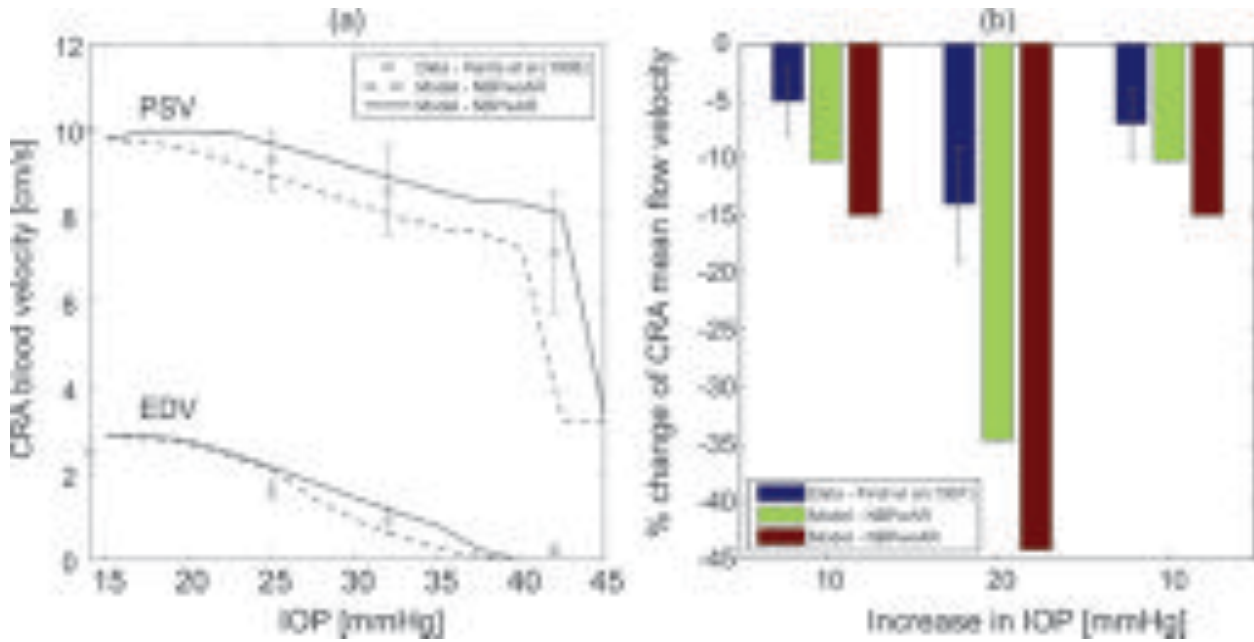
346 **Clinical data and theoretical predictions.** The mathematical model is used to
 347 aid the interpretation of clinically measured hemodynamic responses to surgical IOP
 348 reduction in glaucoma patients and induced IOP elevation in healthy individuals.

349 *Surgical IOP reduction on glaucoma patients.* Galassi et al.⁹ and Trible et al.¹⁴
 350 report an increase in CRA blood velocity and a decrease in RI following trabeculectomy
 351 (group (a) in Galassi et al. and Trible et al.) and deep sclerectomy (group (b) in Galassi
 352 et al.), as indicated by the changes (Δ) in MFV, PSV, EDV and RI summarized in Table
 353 6. Since the study by Trible et al.¹⁴ reports MAP values of 107 ± 14.7 mmHg, we use
 354 HBP-model predictions that correspond to MAP = 106.7 mmHg as a comparison with
 355 clinical data. Also, to be consistent with the data, model simulations assume that IOP =
 356 30 mmHg before surgery and IOP = 15 mmHg after surgery. The model assumptions
 357 have been indicated with shaded boxes in Table 6. Model predicted values of Δ MFV,

358 ΔPSV , ΔEDV and ΔRI for the HBPwoAR case and the trabeculectomy data reported by
359 Trible et al.¹⁴ differ only by 0.3 cm/s, 0.38 cm/s, 0.58 cm/s and 0.01, respectively. The
360 model predicted values of ΔEDV and ΔRI for the HBPwAR and HBPwoAR cases and
361 the deep sclerectomy data reported by Galassi et al.⁹ (group (b)) also show the same
362 qualitative trends.

363 *Induced IOP elevation on healthy individuals.* The model predicted values of PSV
364 and EDV in the CRA for IOP between 15 and 45 mmHg are compared with the clinical
365 data by Harris et al.¹⁰ in Figure 8(a). In the study by Harris et al., PSV and EDV
366 measurements were performed at an intermediate location between the lamina cribrosa
367 and the eye globe, corresponding to the intraocular CRA segment of our model. Since
368 the study involved healthy individuals, the clinical data are compared with the
369 NBP-model predictions. Figure 8(a) shows that the PSV values measured by Harris et al.
370 and predicted by our model in the NBP- case fall precisely in the same range.

371 The model-predicted values of percent change in the CRA mean flow velocity with
372 IOP elevation are compared with the clinical data by Findl et al.⁸ in Figure 8(b). In the
373 study by Findl et al., IOP was raised 20 mmHg above baseline in two steps and then was
374 reduced by 10 mmHg before releasing the suction cup. Measurements were performed
375 at approximately 3 mm behind the optic disc surface, corresponding to the retrobulbar
376 CRA segment in our model. Findl et al. considered healthy individuals and therefore
377 the clinical data are compared with the NBP- model predictions.



378

379 **Figure 8:** (a) Comparison between peak systolic velocity (PSV) and end diastolic
 380 velocity (EDV) measured by Harris et al.¹⁰ in the central retinal artery (CRA) and the
 381 model predicted values in the NBPwAR and NBPwoAR cases. (b) Comparison between
 382 the percent change in CRA mean flow velocity measured by Findl et al.⁸ and the model
 383 predicted values in the NBPwAR and NBPwoAR cases.

384

385 **4 Discussion**

386 The combination of multiple factors, including IOP, BP and autoregulation, plays a
 387 primary role in determining retinal and retrobulbar hemodynamics. It is widely
 388 recognized that IOP elevation poses a serious challenge to tissue perfusion, and several
 389 animal and human studies, in addition to the results of the theoretical model presented
 390 here, have suggested that arterial blood pressure^{2, 28-32} and blood flow autoregulation^{2,}
 391 ³³⁻³⁵ are also important factors influencing blood flow. However, the difficulty of isolating
 392 and assessing the contributions of arterial blood pressure and blood flow autoregulation
 393 *in vivo* limits the current understanding of their effects on tissue perfusion as IOP
 394 varies²⁸. The current study introduces a mathematical model that can serve as a virtual
 395 lab where the contributions of arterial blood pressure and blood flow autoregulation can

396 be isolated and their influence on the tissue susceptibility to IOP challenge can be
397 predicted and assessed independently.

398 **Model validation.** Every mathematical model is based on simplifying
399 assumptions whose validity needs to be verified by comparing model predictions with
400 data from independent experimental and clinical studies. Figure 4 shows that the model
401 predicted values of velocity and flow are consistent with clinical measurements^{63, 69-71, 77,}
402 ⁷⁸. These measurements were used for comparison purposes only and were not used to
403 estimate any of the model parameters listed in Tables 1, 4, 7, 8 and 9. It is important to
404 note that many of the model parameters vary among individuals. In particular, many
405 studies have shown that the geometric and mechanical properties of the lamina cribrosa
406 and sclera undergo change with age^{41, 42}, ethnicity^{36, 79} and disease^{47, 48}, and these
407 changes strongly affect the biomechanical response of the optic nerve head tissues to
408 IOP alterations⁵⁰⁻⁵⁶. The clinical studies^{63, 69-71, 77, 78} used for model comparison did not
409 report the parameter values for the geometric and mechanical properties of the lamina
410 cribrosa and sclera, and therefore the model simulations were performed using the
411 literature-based parameter choice reported in Tables 7 and 8. Future data on the
412 geometric and structural properties of the retinal vessels collected from populations of a
413 wide age range will help to improve upon the current model predictions.

414 Despite the simplified vascular architecture and the literature-based parameter
415 choice, the model predictions of velocity and flow reported in Figure 4 are consistent with
416 six independent clinical studies, providing evidence that our modeling choices are
417 appropriate and physiologically reasonable.

418 **Theoretical investigations.** The model simulations suggest that the

419 hemodynamic response of the retinal vasculature to IOP variations noticeably differ
420 among individuals with different blood pressure and functionality of autoregulation.

421 *Total retinal blood flow.* The model predicts that the autoregulation plateau would
422 shift towards higher IOP values as MAP increases, as shown in Figure 6. This is in
423 agreement with the study by He et al.³⁰, who induced IOP elevations on Long-Evan rats
424 with low, moderate, and high MAP levels and found that a higher IOP was needed to
425 attenuate ocular blood flow in animals with higher MAP. The shift in the autoregulation
426 plateau was also predicted by the theoretical work of Arciero et al.⁶¹, whose
427 microcirculation model suggested that autoregulation fails to operate over its expected
428 range of arterial pressure if IOP is increased.

429 *CRA blood velocity.* The model predicts that the blood flow velocity in the CRA
430 does not always decrease with IOP elevation. Figures 5(b) and 5(c) show a slight
431 increase in PSV in the range of IOP values for which autoregulation is achieved, namely
432 between 15 and 23 mmHg for NBPwAR and between 23 and 29 mmHg for HBPwAR.

433 These findings have important clinical implications. For example, the model
434 suggests that a 10 mmHg IOP reduction in an individual with normal blood pressure and
435 functional autoregulation (NBPwAR) would result in a noticeable increase in PSV and
436 EDV in the CRA blood velocity and a noticeable increase in total retinal blood flow if IOP
437 is reduced from 40 to 30 mmHg. However, only minimal hemodynamic changes are
438 predicted if IOP is reduced from 25 to 15 mmHg. These findings could help to explain
439 why some studies^{9, 13, 14} report significant hemodynamic changes following
440 trabeculectomy, while others do not^{17, 24}. The model also suggests that IOP reductions of
441 approximately 5 mmHg would result in minor hemodynamic changes in all the cases

442 considered here, which is consistent with clinical data related to topical medications^{7, 11,}
443 ^{12, 15, 16, 19-23, 25-27}. However, reductions in IOP greater than 5 mmHg may have a more
444 significant effect on retinal hemodynamics. The hypotensive effects of prostaglandin
445 analogues, combination therapies and surgical interventions may far exceed this
446 threshold depending on the patient's IOP level prior to medical intervention.

447 *Intraluminal blood pressure.* Intraluminal blood pressure is the main driving force
448 of local tissue perfusion and can be measured in retinal vessels by artificially increasing
449 IOP using ophthalmodynamometry⁸⁰⁻⁸³. However, the level of IOP may have an
450 important impact on the intraluminal pressure in retinal vessels, which is uncovered by
451 the mathematical model. The model predicts that increased IOP induces a significant
452 increase in the intraluminal blood pressure in all vascular compartments upstream of the
453 CRV. This finding is consistent with the experimental observations by Gluksberg and
454 Dunn⁸⁴ and Attariwala et al⁸⁵ on live anesthetized cats. A hydraulic feedback mechanism
455 could explain this phenomenon^{84, 85}. Veins are more susceptible than arteries to IOP
456 elevation, since veins have thinner walls and lower intraluminal pressure than arteries
457 and, under extreme conditions, act like a Starling resistor and collapse. Thus, as IOP
458 increases, resistance to flow increases in veins more than in arteries, leading to an
459 overall increase in intraluminal pressure upstream of the veins^{86, 87}. In addition, the
460 model predicts that IOP elevation would affect intraluminal arterial pressure differently
461 depending on whether blood flow autoregulation is functional or absent. The study by
462 Jonas⁸³ supports this finding, since correlation coefficients between intraluminal blood
463 pressure measured via ophthalmodynamometry and systemic blood pressure were
464 found lower in eyes with retinal or orbital diseases than in the control group.

465 **Clinical data and theoretical predictions.** A good qualitative and quantitative
466 agreement in the hemodynamic response to IOP changes was found between clinical
467 data and model predictions. This suggests that the mathematical model could be used to
468 anticipate the hemodynamic outcome of clinical IOP modulation on specific patients.

469 *Surgical IOP reduction on glaucoma patients.* The clinical studies by Galassi et
470 al.⁹ and Trible et al.¹⁴ suggest that clinically measurable changes in the retinal
471 hemodynamic parameters occur in patients with elevated blood pressure as IOP is
472 reduced from 30 to 15 mmHg. The theoretical analysis in the current study suggests that
473 these changes are less pronounced in HBPwAR patients than in HBPwoAR patients,
474 likely due to the compensatory mechanisms of autoregulation⁸⁸. However, the model
475 also suggests that if a 15 mmHg IOP reduction falls within the regulating range predicted
476 for HBP-patients, the consequent hemodynamic changes would be negligible. This might
477 explain why the trabeculectomy study by Cantor¹⁷ did not observe any significant change
478 in ocular blood flow parameters despite significant IOP reduction.

479 *Induced IOP elevation on healthy individuals.* The ability to autoregulate blood
480 flow has a noticeable effect in individuals with normal blood pressure experiencing
481 induced IOP elevation. Figure 8(a) shows good agreement between clinical data and
482 model predictions in the NBPwoAR case when IOP is increased. Blood velocity
483 measurements were performed immediately after IOP elevation (i.e., before
484 autoregulation took effect), explaining why the NBPwoAR model predictions match the
485 data more closely than the NBPwAR predictions. Consistent with this interpretation,
486 there is better agreement between the data and the NBPwAR case in Figure 8(b) since

487 the blood velocity measurements were performed at least 5 minutes after IOP elevation,
488 leaving time for autoregulation to exert its influence.

489 **Limitations of the present model.** In the model, the geometrical architecture of
490 the retinal vasculature is reduced to five main compartments which do not account for
491 the three-dimensional spatial arrangements of the vessels. An extension of the model to
492 more realistic geometries could help to uncover hemodynamic differences observed
493 among nasal, temporal, superior and inferior retinal quadrants⁸⁹. Currently, blood flow
494 autoregulation is modeled only phenomenologically as the ability of retinal arterioles to
495 alter their resistance to maintain relatively constant blood flow over a certain pressure
496 range. Expanding the model to incorporate a mechanistic autoregulation description,
497 such as the one developed by Arciero et al.⁶¹, could help to investigate the hemodynamic
498 consequences of IOP alterations in subjects who suffer from metabolic¹ or endothelial⁹⁰
499 dysfunction. Employing the mechanistic autoregulation description will also very likely
500 increase the current pressure range for which autoregulation is predicted to function.
501 The current autoregulation range of about 8-10 mmHg is not consistent with the larger
502 autoregulation plateaus observed clinically. Implementing the model for a more realistic
503 network geometry instead of lumping all arterioles into a single compartment will also
504 help to yield a larger autoregulation plateau. Finally, the lamina cribrosa is assumed to
505 be circular, isotropic and homogeneous, while its geometrical and mechanical properties
506 are much more complex^{45, 49} and vary with age^{41, 42}, ethnicity^{36, 79} and disease^{47, 48}. The
507 model could be extended to include a more realistic description of the lamina cribrosa to
508 allow for a more accurate evaluation of the effects of aging, racial differences and
509 diseases on the relationship between IOP and blood flow.

510 **Concluding remarks.** Despite its several underlying assumptions, the
511 mathematical model developed in this study offers the first theoretical framework
512 capable of linking the mechanical action of IOP to clinically measurable hemodynamic
513 quantities, such as total retinal blood flow and CRA blood velocity. Model simulations are
514 used to assess the independent effects of varying arterial blood pressure (BP) and blood
515 flow autoregulation (AR) on the relationship between IOP and blood flow.

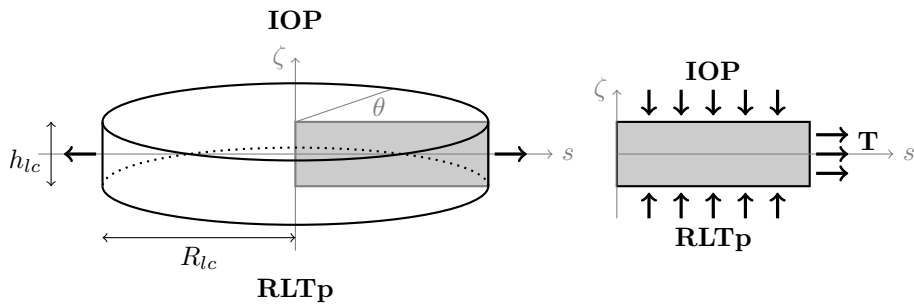
516 Studies have generally not examined the respective roles of BP and AR on flow
517 due to the difficulty in isolating and evaluating these two factors clinically. Our
518 mathematical model, which is validated with clinically attained values of retinal blood flow
519 and velocity, is used to predict how BP levels (high, normal or low) and AR ability
520 (functional or absent) affect retinal blood flow in response to changes in IOP. Because
521 our model predictions are consistent with clinical data for IOP-reduction via surgery and
522 medications, as well as for induced IOP-elevation, this investigation represents a first
523 attempt to use a patient's BP and AR to more accurately predict how a patient's retinal
524 blood flow may or may not be influenced by clinically altered IOP levels. A better
525 understanding of this relationship could have important implications for improving the
526 way that we therapeutically address diseases associated with retinal blood flow,
527 including glaucoma¹⁻³, age-related macular degeneration^{4, 5} and diabetes^{5, 6}.

528

529 **5 Appendix**

530 **IOP-induced stress in the lamina cribrosa.** The lamina cribrosa is modeled as
531 a nonlinear, homogeneous, isotropic, elastic circular plate of radius R_{lc} and finite
532 thickness h_{lc} , satisfying the equilibrium equation $\nabla \cdot \mathbf{S} = \mathbf{0}$, where $\mathbf{S} = \lambda_{lc}(\sigma_e)tr(\mathbf{E})\mathbf{I} +$

533 $2\mu_{lc}(\sigma_e)\mathbf{E}$ is the stress tensor, $\mathbf{E} = [\nabla\mathbf{u} + (\nabla\mathbf{u})^T + (\nabla\mathbf{u})^T\nabla\mathbf{u}]/2$ is the Green-Saint
 534 Venant strain tensor, \mathbf{u} is the displacement vector, μ_{lc} is the shear modulus, $\lambda_{lc} =$
 535 $\mu_{lc}(E_{lc} - 2\mu_{lc})/(3\mu_{lc} - E_{lc})$ is the Lame's parameter, and E_{lc} is the Young's modulus.
 536 The elastic parameters λ_{lc} and μ_{lc} vary with the effective stress σ_e , as described by
 537 Guidoboni et al.^{36, 62}. The problem is solved in cylindrical coordinates, as shown in Figure
 538 9 with the boundary conditions $\mathbf{S}\mathbf{n} = -\text{IOP}\mathbf{n}$ at $\zeta = h/2$, $\mathbf{S}\mathbf{n} = -\text{RLTp}\mathbf{n}$ at $\zeta = -h/2$, $\mathbf{n}\mathbf{S}\mathbf{n} =$
 539 T and $u_\zeta = 0$ at $s = R_{lc}$, where T is the scleral tension computed via Laplace's law $T =$
 540 $\text{IOP } R_s / 2h_s$, where R_s and h_s are the radius and thickness of the sclera, respectively.
 541 Geometrical and mechanical properties of the lamina and sclera are summarized in
 542 Tables 7 and 8; the numerical solution of the elastic problem via finite elements is
 543 described in reference⁶². The radial component of the normal stress S_{ss} at $s=0$ resulting
 544 from the solution of this elastic problem is assumed to be the external pressure acting on
 545 the intralaminar segments of the CRA and CRV, which are assumed to pierce the lamina
 546 in its center⁶².



547
 548 **Figure 9:** Schematic representation of geometry and boundary conditions of the
 549 elasticity problem for the lamina cribrosa. The anterior surface ($\zeta = h_{lc}/2$) is subject to the
 550 intraocular pressure (IOP), while the posterior surface ($\zeta = -h_{lc}/2$) is subject to the
 551 retrolaminar tissue pressure (RLTp). The lateral surface ($s = R_{lc}$) is connected to the
 552 sclera and experiences the scleral tension T .

553 **Passive variable resistances.** The vascular resistance of a blood vessel can be

554 obtained by combining a tube law, describing the mechanical response of the vessel wall
 555 to changes in transmural pressure ΔP , and a hydrodynamic law, describing the fluid flow
 556 through the tube.

557 In the case of arteries, the Law of Laplace is used to describe a pressurized
 558 cylindrical shell and Poiseuille's law is used to describe fluid flow through the vessel.
 559 As a result, CRA resistance varies according to:

$$R = \frac{k_r \rho L}{A_{ref}^2} \left(1 + \frac{\Delta P}{k_p k_L}\right)^{-4} \quad (2)$$

560 with $k_r = \frac{8\pi\mu}{\rho}$, where μ and ρ are the fluid viscosity and density, respectively;

561 $k_p = \frac{Eh^3}{\sqrt{1-\nu^2}} \left(\frac{\pi}{A_{ref}}\right)^{\frac{3}{2}}$, where E , ν and h are the Young's modulus, the Poisson's ratio and the
 562 thickness of the vessel wall, respectively; A_{ref} is the vessel cross-sectional area when
 563 $\Delta P = 0$ (assumed to be circular); and $k_L = \frac{12A_{ref}}{\pi h^2}$.

564 In venules and veins, the trasmural pressure difference may become negative,
 565 causing the vessel to collapse. This phenomenon, known as a Starling resistor, is
 566 modeled here by replacing the Law of Laplace with a more realistic tube law⁹¹ that allows
 567 for drastic changes in the cross sectional area when $\Delta P < 0$. Resistance is thus
 568 calculated as:

$$R = \begin{cases} \frac{k_r \rho L}{A_{ref}^2} \left(1 + \frac{\Delta P}{k_p k_L}\right)^{-4} & \text{for } \Delta P \geq 0 \\ \frac{k_r \rho L}{A_{ref}^2} \left(1 - \frac{\Delta P}{k_p}\right)^{4/3} & \text{for } \Delta P < 0 \end{cases} \quad (3)$$

569 where the values for Young's modulus, Poisson's ratio, and the wall-to-lumen ratio are
 570 provided in Table 9. It is worth noticing that changes in ΔP can be due to variations in

571 the external pressure and/or intraluminal blood pressure. Equation (2) is used for the
572 segment 1d with external pressure equal to IOP, and the segment 1c with an external
573 pressure that depends on the IOP-induced stress in the lamina cribrosa⁶². Equation (3) is
574 used for segments 4a, 4b, and 5a with external pressure equal to IOP, and for the
575 segment 5b with an external pressure that depends on the IOP-induced stress in the
576 lamina cribrosa.

577 **Active variable resistances.** Blood flow autoregulation relies on the adaptation
578 of the vascular tone of resistance vessels to changes in the perfusion pressure or
579 metabolic needs of the tissue. Recently, Arciero et al⁶¹ have developed a mathematical
580 model that describes the response of resistance vessels to local changes in pressure,
581 shear stress, carbon dioxide and to the downstream metabolic state communicated via
582 conducted responses. The model is based on a mechanical representation of resistance
583 vessel walls where the total circumferential wall tension is generated by a passive
584 component (representing the wall tension generated by the structural components of the
585 vessel wall) and an active component (representing the wall tension generated in
586 response to changes in smooth muscle tone). A stimulus function is defined to describe
587 changes in smooth muscle tone according to a linear combination of various regulatory
588 mechanisms.

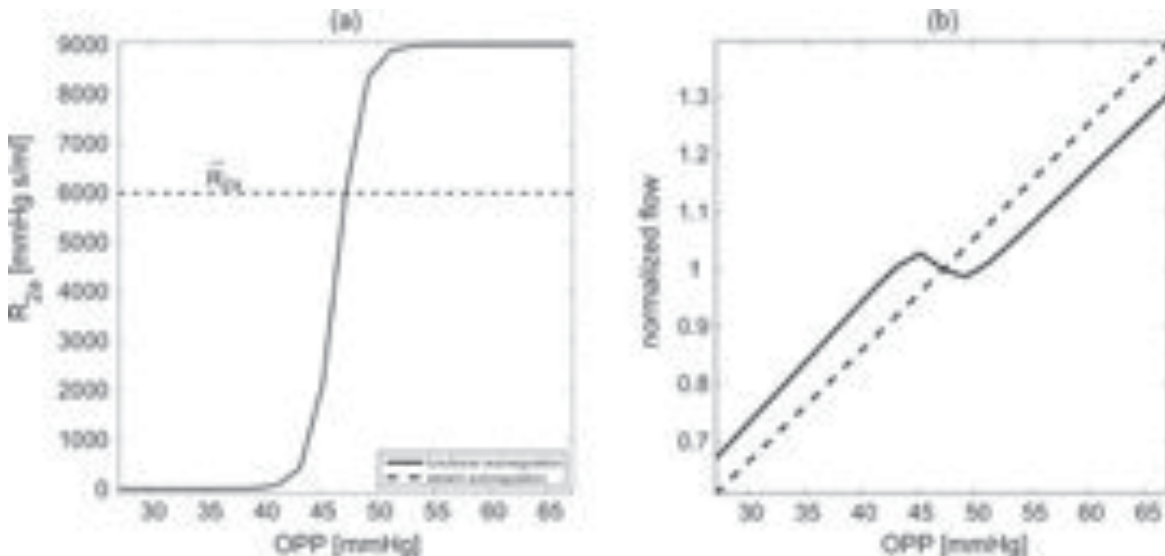
589 The model proposed by Arciero et al. cannot be directly coupled with the model
590 for retinal blood flow developed in the present article, since the first model is stationary
591 while the second model is time-dependent. The extension of the model by Arciero et al.
592 to the time-dependent case would require the description of the mechanisms regulating
593 retinal blood flow in response to time variations of intravascular pressures, blood velocity

594 and shear stress, which, while beyond the scope of this paper, we acknowledge as a
595 limitation in the current manuscript.

596 Thus, here we adopt a simpler phenomenological description of blood flow
597 autoregulation, following the method utilized by Lakin et al. in the context of cerebral
598 blood flow⁷⁶. The absence of autoregulation is modeled by keeping the arteriolar
599 resistance R_{2a} constantly equal to its control value \bar{R}_{2a} despite changes in ocular
600 perfusion pressure (OPP), while functional autoregulation is modeled by letting arteriolar
601 resistance vary according to the formula:

$$R_{2a} = R_{2b} = \bar{R}_{2a} \frac{c_L + c_U \exp[K(Q_{noAR}(OPP) - \bar{Q}) - \hat{c}]}{1 + \exp[K(Q_{noAR}(OPP) - \bar{Q}) - \hat{c}]} \quad (3)$$

602 where $c_L = 2.50 \cdot 10^{-3}$ and $c_U = 1.5$ determine the lower and upper bounds for the
603 variation in resistance, $K = 6.91 \cdot 10^4$ s/ml determines the resistance sensitivity to
604 changes in OPP (= 2/3 MAP - IOP), $Q_{noAR}(OPP)$ is the total retinal blood flow predicted
605 by the model in the absence of autoregulation for a given OPP and $\hat{c} = \ln(c_U - 1) -$
606 $\ln(1 - c_L)$ ensures that $R_{2a} = \bar{R}_{2a}$ and $R_{2b} = \bar{R}_{2b}$ at the control state. The numerical
607 values of c_L , c_U and K have been chosen to yield an increase in resistance over the
608 range of OPP depicted in Figure 10(a). Model simulations of normalized flow in the
609 case of functional and absent autoregulation are reported in Figure 10 (b) for various
610 OPP values (attained by setting IOP = 15 mmHg and varying MAP between 63 and 123
611 mmHg).



612

613 **Figure 10:** Arteriolar resistance (a) and normalized flow (b) for model simulations with
 614 functional (solid line) or absent (dashed line) autoregulation for various ocular perfusion
 615 pressures (OPP) attained by setting IOP = 15mmHg and varying MAP.

616

617 Figure 4(c) shows that the model predicted values of retinal blood flow in the case of
 618 functional autoregulation are consistent with clinical measurements for various MAP
 619 levels, and this suggests that formula (3) and its related assumptions are appropriate
 620 modeling choices for retinal blood flow autoregulation.

621

622 Acknowledgements

623 This work has been partially supported by the NSF DMS-1224195,
 624 NIH1R21EY022101-01A1 and the Indiana University Collaborative Research Grant of
 625 the Office of the Vice President for Research.

626 Tables

627 Table 1: Geometric and physical parameters for the central retinal artery (CRA) and
 628 central retinal vein (CRV).

Parameters	CRA		CRV	
	Value	Source	Value	Source
Diameter D [μm]	175	Dorner et al. ⁶⁸	238	Takahashi et al. ⁶⁰ , (a)

Length L [mm]	<i>total</i>	10	Harris et al. ⁹²	10	Harris et al. ⁹²
	<i>segment a</i>	4.4	Harris et al. ⁹²	1	Lee et al. ⁹³
	<i>segment b</i>	4.4	Harris et al. ⁹²	0.2	Jonas et al. ⁹⁴ Ren et al. ⁹⁵
	<i>segment c</i>	0.2	Jonas et al. ⁹⁴ Ren et al. ⁹⁵	4.4	Harris et al. ⁹²
	<i>segment d</i>	1	Lee et al. ⁹³	4.4	Harris et al. ⁹²
Blood viscosity μ [cP]		3.0	Fung ⁹⁶ Quarteroni et al. ⁹⁷	3.24	Takahashi et al. ⁶⁰ , (b)
Wall Young's Modulus E [MPa]		0.3	Armentano et al. ⁹⁸ Fung ⁹⁹ Quarteroni et al. ⁹⁷	0.6	Deng et al. ¹⁰⁰
Wall Poission's ratio ν [1]		0.49	Armentano et al. ⁹⁸ Fung ⁹⁹ Quarteroni et al. ⁹⁷	0.49	(c)
Wall Thickness h [μm]		39.7	Baleanu et al. ¹⁰¹	10.7	Wetterer et al. ¹⁰²

- 629 (a) CRA/CRV diameter ratio is assumed to be the same as that for the first generation
 630 arteries/veins in the model by Takahashi et al.⁶⁰.
 631 (b) Blood viscosity in the CRV is assumed to be 8% larger than that in the CRA as in the
 632 model by Takahashi et al.⁶⁰.
 633 (c) Poisson's ratio of the CRV wall is assumed to be the same as that for the CRA wall.

634

635

636

637 Table 2: Computed values of the vascular resistances at the control state

Resistance	Value [mmHg s/ml]	Resistance	Value [mmHg s/ml]
\bar{R}_{in}	$2.25 \cdot 10^4$	\bar{R}_{3b}	$5.68 \cdot 10^3$
\bar{R}_{1a}	$4.30 \cdot 10^3$	\bar{R}_{4a}	$3.11 \cdot 10^3$
\bar{R}_{1b}	$4.30 \cdot 10^3$	\bar{R}_{4b}	$3.11 \cdot 10^3$
\bar{R}_{1c}	$1.96 \cdot 10^2$	\bar{R}_{5a}	$3.08 \cdot 10^2$
\bar{R}_{1d}	$9.78 \cdot 10^2$	\bar{R}_{5b}	$6.15 \cdot 10^1$
\bar{R}_{2a}	$6.00 \cdot 10^3$	\bar{R}_{5c}	$1.35 \cdot 10^3$
\bar{R}_{2b}	$6.00 \cdot 10^3$	\bar{R}_{5d}	$1.35 \cdot 10^3$
\bar{R}_{3a}	$5.68 \cdot 10^3$	\bar{R}_{out}	$5.74 \cdot 10^3$

638

639

640

641

642

643 Table 3: Computed values of intraluminal blood pressures at the control state

Pressure	Value [mmHg]	Pressure	Value [mmHg]
\bar{P}_{in}	62.22	$\bar{P}_{3,4}$	24.25
$\bar{P}_{1,in}$	46.85	\bar{P}_4	22.13
\bar{P}_1	43.92	$\bar{P}_{4,5}$	20.01
$\bar{P}_{1,pre}$	40.99	$\bar{P}_{5,post}$	19.80

$\bar{P}_{1,post}$	40.85	$\bar{P}_{5,pre}$	19.76
$\bar{P}_{1,2}$	40.19	\bar{P}_5	18.84
\bar{P}_2	36.09	$\bar{P}_{5,out}$	17.92
$\bar{P}_{2,3}$	32.00 (a)	\bar{P}_{out}	14.00
\bar{P}_3	28.13		

644 (a) This value has chosen on the bases of previous studies by Arciero et al.⁶¹ and
 645 Friedland⁷⁴.

646

647

648

649 Table 4: Computed values of volumes and capacitances at the control state

Segment	Volume [ml]	Capacitance C [ml/mmHg]
CRA	$2.12 \cdot 10^{-4}$	$7.22 \cdot 10^{-7}$
Arterioles	$2.20 \cdot 10^{-4}$	$7.53 \cdot 10^{-7}$
Venules	$6.12 \cdot 10^{-4}$	$1.67 \cdot 10^{-5}$
CRV	$3.92 \cdot 10^{-4}$	$1.07 \cdot 10^{-5}$

650

651

652 Table 5: Representative cases for model simulations. The cases represent individuals
 653 with normal, high and low arterial blood pressure (NBP-, HBP-, LBP-) and with functional
 654 or absent blood flow autoregulation (-wAR, -woAR)

Case	Description
HBP-	Systolic/diastolic blood pressure = 140/90 mmHg
NBP-	Systolic/diastolic blood pressure = 120/80 mmHg
LBP-	Systolic/diastolic blood pressure = 100/70 mmHg
-wAR	Variable arteriolar resistances, see equation (3) in Appendix
-woAR	Fixed arteriolar resistances, kept at control values

655

656

657

658

659 Table 6: Changes in peak systolic velocity (PSV), end diastolic velocity (EDV), resistivity
 660 index (RI) and mean flow velocity (MFV) in the central retinal artery as IOP is reduced by
 661 trabeculectomy (group (a) in Galassi et al⁹ and Trible et al¹⁴), deep sclerectomy (group
 662 (b) in Galassi et al⁹) and model simulations. Model assumptions are reported in shaded
 663 boxes.

664

Parameter	Clinical Studies			Mathematical Model	
Study	<i>Galassi et al</i> ⁹ group (a)	<i>Galassi et al</i> ⁹ group (b)	<i>Tribble et al</i> ¹⁴	<i>HBPwAR</i>	<i>HBPwoAR</i>
Pre-op IOP [mmHg]	25.27±6.24	24.05±4.27	27.5±8.8	30	30
Post-op IOP [mmHg]	9.86±2.10	10.79±2.27	12.5±10.5	15	15
Pre-op MAP [mmHg]	-	-	107±14.7	106.7	106.7
Post-op MAP [mmHg]	-	-	102.2±11.5	106.7	106.7
Δ MFV [cm/s]	-	-	1.4	1.0	1.7
Δ PSV [cm/s]	-	-	1.2	-0.13	1.58
Δ EDV [cm/s]	0.40	0.47	0.96	1.33	1.54
Δ RI [1]	-0.06	-0.05	-0.12	-0.13	-0.11

665

666 Table 7: Radius and thickness values used in the mathematical model for the lamina
667 cribrosa and sclera

Parameter	Value	Source
Radius of the lamina cribrosa R_{lc} [mm]	0.75	<i>Jonas et al</i> ¹⁰³
Thickness of the lamina cribrosa h_{lc} [mm]	0.2	<i>Jonas et al.</i> ⁹⁴ <i>Ren et al.</i> ⁹⁵
Radius of the sclera R_s [mm]	12	<i>Jonas et al.</i> ⁹⁴ <i>Norman et al.</i> ¹⁰⁴
Thickness of the sclera h_{lc} [mm]	1	<i>Norman et al.</i> ¹⁰⁴ <i>Ren et al.</i> ⁹⁵

668

669 Table 8: Model values of Young's modulus E_{lc} and shear modulus μ_{lc} for the lamina
670 cribrosa as a function of the effective stress σ_e , as in *Newson et al.*¹⁰⁵ and *Woo et al.*¹⁰⁶

E_{lc} [MPa]	μ_{lc} [MPa]	Range of σ_e [MPa]
0.358	0.12	0.008 > $\sigma_e \geq 0.000$
0.656	0.22	0.015 > $\sigma_e \geq 0.008$
1.818	0.61	$\sigma_e \geq 0.015$

671

672

673 Table 9: Physical parameters for the arterioles and venules

Parameter	Arterioles	Venules
Wall Young's Modulus E [MPa]	0.022	0.066
Wall Poission's ratio ν [1]	0.49	0.49
Wall-to-Lumen ratio	0.23	0.05

674

675

References

- 676 1. Harris A, Kagemann L, Ehrlich R, Rospigliosi C, Moore D, Siesky B. Measuring and
677 interpreting ocular blood flow and metabolism in glaucoma. *Canadian journal of ophthalmology*
678 *Journal canadien d'ophthalmologie* 2008;43:328-336.

- 679 2. Leske MC. Open-angle glaucoma -- an epidemiologic overview. *Ophthalmic*
680 *epidemiology* 2007;14:166-172.
- 681 3. Leske MC, Heijl A, Hyman L, Bengtsson B, Dong L, Yang Z. Predictors of long-term
682 progression in the early manifest glaucoma trial. *Ophthalmology* 2007;114:1965-1972.
- 683 4. Ehrlich R, Harris A, Kheradiya NS, Winston DM, Ciulla TA, Wirostko B. Age-related
684 macular degeneration and the aging eye. *Clinical interventions in aging* 2008;3:473-482.
- 685 5. Pemp B, Schmetterer L. Ocular blood flow in diabetes and age-related macular
686 degeneration. *Canadian journal of ophthalmology Journal canadien d'ophtalmologie*
687 2008;43:295-301.
- 688 6. Rassam SM, Patel V, Kohner EM. The effect of experimental hypertension on retinal
689 vascular autoregulation in humans: a mechanism for the progression of diabetic retinopathy.
690 *Experimental physiology* 1995;80:53-68.
- 691 7. Alagoz G, Gurel K, Bayer A, Serin D, Celebi S, Kukner S. A comparative study of
692 bimatoprost and travoprost: effect on intraocular pressure and ocular circulation in newly
693 diagnosed glaucoma patients. *Ophthalmologica Journal international d'ophtalmologie*
694 *International journal of ophthalmology Zeitschrift fur Augenheilkunde* 2008;222:88-95.
- 695 8. Findl O, Strenn K, Wolzt M, et al. Effects of changes in intraocular pressure on human
696 ocular haemodynamics. *Current eye research* 1997;16:1024-1029.
- 697 9. Galassi F, Giambene B, Corvi A, Falaschi G, Menchini U. Retrobulbar hemodynamics and
698 corneal surface temperature in glaucoma surgery. *International ophthalmology*
699 2008;28:399-405.
- 700 10. Harris A, Joos K, Kay M, et al. Acute IOP elevation with scleral suction: effects on
701 retrobulbar haemodynamics. *The British journal of ophthalmology* 1996;80:1055-1059.
- 702 11. Huber-van der Velden KK, Lux A, Severing K, Klamann MK, Winterhalter S, Remky A.
703 Retrobulbar hemodynamics before and after oculopression with and without dorzolamide.
704 *Current eye research* 2012;37:719-725.
- 705 12. Koz OG, Ozsoy A, Yarangumeli A, Kose SK, Kural G. Comparison of the effects of
706 travoprost, latanoprost and bimatoprost on ocular circulation: a 6-month clinical trial. *Acta*
707 *ophthalmologica Scandinavica* 2007;85:838-843.
- 708 13. Synder A, Augustyniak E, Laudanska-Olszewska I, Wesolek-Czernik A. [Evaluation of
709 blood-flow parameters in extraocular arteries in patients with primary open-angle glaucoma
710 before and after surgical treatment]. *Klinika oczna* 2004;106:206-208.
- 711 14. Trible JR, Sergott RC, Spaeth GL, et al. Trabeculectomy is associated with retrobulbar
712 hemodynamic changes. A color Doppler analysis. *Ophthalmology* 1994;101:340-351.
- 713 15. Akarsu C, Yilmaz S, Taner P, Ergin A. Effect of bimatoprost on ocular circulation in
714 patients with open-angle glaucoma or ocular hypertension. *Graefe's archive for clinical and*
715 *experimental ophthalmology = Albrecht von Graefes Archiv fur klinische und experimentelle*
716 *Ophthalmologie* 2004;242:814-818.
- 717 16. Arikan OK, Akarsu C, Unal B, Ergin A, Koc C. Effect of oxymetazoline nasal spray on
718 intraocular pressure and retrobulbar hemodynamics. *The Journal of otolaryngology*
719 2006;35:30-35.
- 720 17. Cantor LB. The effect of trabeculectomy on ocular hemodynamics. *Transactions of the*
721 *American Ophthalmological Society* 2001;99:241-252.
- 722 18. Conway ML, Wevill M, Benavente-Perez A, Hosking SL. Ocular blood-flow

- 723 hemodynamics before and after application of a laser in situ keratomileusis ring. *Journal of*
724 *cataract and refractive surgery* 2010;36:268-272.
- 725 19. Erkin EF, Tarhan S, Kayikcioglu OR, Deveci H, Guler C, Goktan C. Effects of betaxolol and
726 latanoprost on ocular blood flow and visual fields in patients with primary open-angle
727 glaucoma. *European journal of ophthalmology* 2004;14:211-219.
- 728 20. Fuchsjager-Mayrl G, Georgopoulos M, Hommer A, et al. Effect of dorzolamide and
729 timolol on ocular pressure: blood flow relationship in patients with primary open-angle
730 glaucoma and ocular hypertension. *Investigative ophthalmology & visual science*
731 2010;51:1289-1296.
- 732 21. Harris A, Garzozi HJ, McCranor L, Rechtman E, Yung CW, Siesky B. The effect of
733 latanoprost on ocular blood flow. *International ophthalmology* 2009;29:19-26.
- 734 22. Hommer A, Sperl P, Resch H, et al. A double-masked randomized crossover study
735 comparing the effect of latanoprost/timolol and brimonidine/timolol fixed combination on
736 intraocular pressure and ocular blood flow in patients with primary open-angle glaucoma or
737 ocular hypertension. *Journal of ocular pharmacology and therapeutics : the official journal of*
738 *the Association for Ocular Pharmacology and Therapeutics* 2012;28:569-575.
- 739 23. Inan UU, Ermis SS, Yucel A, Ozturk F. The effects of latanoprost and brimonidine on
740 blood flow velocity of the retrobulbar vessels: a 3-month clinical trial. *Acta ophthalmologica*
741 *Scandinavica* 2003;81:155-160.
- 742 24. James CB. Effect of trabeculectomy on pulsatile ocular blood flow. *The British journal of*
743 *ophthalmology* 1994;78:818-822.
- 744 25. Kaup M, Plange N, Niegel M, Remky A, Arend O. Effects of brinzolamide on ocular
745 haemodynamics in healthy volunteers. *The British journal of ophthalmology* 2004;88:257-262.
- 746 26. Poinoosawmy D, Indar A, Bunce C, Garway-Heath DF, Hitchings RA. Effect of treatment
747 by medicine or surgery on intraocular pressure and pulsatile ocular blood flow in
748 normal-pressure glaucoma. *Graefe's archive for clinical and experimental ophthalmology =*
749 *Albrecht von Graefes Archiv fur klinische und experimentelle Ophthalmologie* 2002;240:721-726.
- 750 27. Stankiewicz A, Misiuk-Hojlo M, Grabska-Liberek I, et al. Intraocular pressure and ocular
751 hemodynamics in patients with primary open-angle glaucoma treated with the combination of
752 morning dosing of bimatoprost and dorzolamide hydrochloride. *Acta ophthalmologica*
753 2011;89:e57-63.
- 754 28. Caprioli J, Coleman AL. Blood pressure, perfusion pressure, and glaucoma. *American*
755 *journal of ophthalmology* 2010;149:704-712.
- 756 29. Hayreh SS, Zimmerman MB, Podhajsky P, Alward WL. Nocturnal arterial hypotension
757 and its role in optic nerve head and ocular ischemic disorders. *American journal of*
758 *ophthalmology* 1994;117:603-624.
- 759 30. He Z, Nguyen CT, Armitage JA, Vingrys AJ, Bui BV. Blood pressure modifies retinal
760 susceptibility to intraocular pressure elevation. *PloS one* 2012;7:e31104.
- 761 31. Leighton DA, Phillips CI. Systemic blood pressure in open-angle glaucoma, low tension
762 glaucoma, and the normal eye. *The British journal of ophthalmology* 1972;56:447-453.
- 763 32. Memarzadeh F, Ying-Lai M, Chung J, Azen SP, Varma R. Blood pressure, perfusion
764 pressure, and open-angle glaucoma: the Los Angeles Latino Eye Study. *Investigative*
765 *ophthalmology & visual science* 2010;51:2872-2877.
- 766 33. Galassi F, Giambene B, Varriale R. Systemic vascular dysregulation and retrobulbar

- 767 hemodynamics in normal-tension glaucoma. *Investigative ophthalmology & visual science*
768 2011;52:4467-4471.
- 769 34. Moore D, Harris A, Wudunn D, Kheradiya N, Siesky B. Dysfunctional regulation of ocular
770 blood flow: A risk factor for glaucoma? *Clin Ophthalmol* 2008;2:849-861.
- 771 35. Sines D, Harris A, Siesky B, et al. The response of retrobulbar vasculature to hypercapnia
772 in primary open-angle glaucoma and ocular hypertension. *Ophthalmic research* 2007;39:76-80.
- 773 36. Guidoboni G, Harris A, Arciero J, et al. Mathematical modeling approaches in the study
774 of glaucoma disparities among people of African and European descents. *J Coupled Syst
775 Multiscale Dyn* 2013;1:21.
- 776 37. Harris A, Guidoboni G, Arciero JC, Amireskandari A, Tobe LA, Siesky BA. Ocular
777 hemodynamics and glaucoma: the role of mathematical modeling. *European journal of
778 ophthalmology* 2013;23:139-146.
- 779 38. Burgoyne CF, Downs JC, Bellezza AJ, Suh JK, Hart RT. The optic nerve head as a
780 biomechanical structure: a new paradigm for understanding the role of IOP-related stress and
781 strain in the pathophysiology of glaucomatous optic nerve head damage. *Progress in retinal and
782 eye research* 2005;24:39-73.
- 783 39. Burgoyne CF. A biomechanical paradigm for axonal insult within the optic nerve head in
784 aging and glaucoma. *Experimental eye research* 2011;93:120-132.
- 785 40. Fazio MA, Grytz R, Bruno L, et al. Regional variations in mechanical strain in the
786 posterior human sclera. *Investigative ophthalmology & visual science* 2012;53:5326-5333.
- 787 41. Fazio MA, Grytz R, Morris JS, et al. Age-related changes in human peripapillary scleral
788 strain. *Biomechanics and modeling in mechanobiology* 2013.
- 789 42. Girard MJ, Suh JK, Bottlang M, Burgoyne CF, Downs JC. Scleral biomechanics in the aging
790 monkey eye. *Investigative ophthalmology & visual science* 2009;50:5226-5237.
- 791 43. Grytz R, Meschke G. Constitutive modeling of crimped collagen fibrils in soft tissues.
792 *Journal of the mechanical behavior of biomedical materials* 2009;2:522-533.
- 793 44. Grytz R, Meschke G. A computational remodeling approach to predict the physiological
794 architecture of the collagen fibril network in corneo-scleral shells. *Biomechanics and modeling
795 in mechanobiology* 2010;9:225-235.
- 796 45. Grytz R, Meschke G, Jonas JB. The collagen fibril architecture in the lamina cribrosa and
797 peripapillary sclera predicted by a computational remodeling approach. *Biomechanics and
798 modeling in mechanobiology* 2011;10:371-382.
- 799 46. Grytz R, Downs JC. A forward incremental prestressing method with application to
800 inverse parameter estimations and eye-specific simulations of posterior scleral shells. *Computer
801 methods in biomechanics and biomedical engineering* 2012.
- 802 47. Grytz R, Sigal IA, Ruberti JW, Meschke G, Downs JC. Lamina Cribrosa Thickening in Early
803 Glaucoma Predicted by a Microstructure Motivated Growth and Remodeling Approach.
804 *Mechanics of materials : an international journal* 2012;44:99-109.
- 805 48. Grytz R, Girkin CA, Libertiaux V, Downs JC. Perspectives on biomechanical growth and
806 remodeling mechanisms in glaucoma(). *Mechanics research communications* 2012;42:92-106.
- 807 49. Grytz R, Fazio MA, Girard MJ, et al. Material properties of the posterior human sclera.
808 *Journal of the mechanical behavior of biomedical materials* 2013.
- 809 50. Norman RE, Flanagan JG, Sigal IA, Rausch SM, Tertinegg I, Ethier CR. Finite element
810 modeling of the human sclera: influence on optic nerve head biomechanics and connections

- 811 with glaucoma. *Experimental eye research* 2011;93:4-12.
- 812 51. Sigal IA, Flanagan JG, Tertinegg I, Ethier CR. Finite element modeling of optic nerve head
813 biomechanics. *Investigative ophthalmology & visual science* 2004;45:4378-4387.
- 814 52. Sigal IA, Flanagan JG, Ethier CR. Factors influencing optic nerve head biomechanics.
815 *Investigative ophthalmology & visual science* 2005;46:4189-4199.
- 816 53. Sigal IA, Ethier CR. Biomechanics of the optic nerve head. *Experimental eye research*
817 2009;88:799-807.
- 818 54. Sigal IA, Flanagan JG, Tertinegg I, Ethier CR. Modeling individual-specific human optic
819 nerve head biomechanics. Part I: IOP-induced deformations and influence of geometry.
820 *Biomechanics and modeling in mechanobiology* 2009;8:85-98.
- 821 55. Sigal IA, Flanagan JG, Tertinegg I, Ethier CR. Modeling individual-specific human optic
822 nerve head biomechanics. Part II: influence of material properties. *Biomechanics and modeling*
823 *in mechanobiology* 2009;8:99-109.
- 824 56. Sigal IA. An applet to estimate the IOP-induced stress and strain within the optic nerve
825 head. *Investigative ophthalmology & visual science* 2011;52:5497-5506.
- 826 57. Ganesan P, He S, Xu H. Development of an image-based network model of retinal
827 vasculature. *Annals of biomedical engineering* 2010;38:1566-1585.
- 828 58. Ganesan P, He S, Xu H. Modelling of pulsatile blood flow in arterial trees of retinal
829 vasculature. *Medical engineering & physics* 2011;33:810-823.
- 830 59. Ganesan P, He S, Xu H. Development of an image-based model for capillary vasculature
831 of retina. *Computer methods and programs in biomedicine* 2011;102:35-46.
- 832 60. Takahashi T, Nagaoka T, Yanagida H, et al. A mathematical model for the distribution of
833 hemodynamic parameters in the human retinal microvascular network. *J Biorheol*
834 2009;23:77-86.
- 835 61. Arciero J, Harris A, Siesky B, et al. Theoretical analysis of vascular regulatory mechanisms
836 contributing to retinal blood flow autoregulation. *Investigative ophthalmology & visual science*
837 2013;54:5584-5593.
- 838 62. Guidoboni G, Harris A, Carichino L, Arieli Y, Siesky B. Effect of intraocular pressure on the
839 hemodynamics of the central retinal artery: a mathematical model. *Math Biosci Eng* In Press.
- 840 63. Harris A, Arend O, Bohnke K, Kroepfl E, Danis R, Martin B. Retinal blood flow during
841 dynamic exercise. *Graefe's archive for clinical and experimental ophthalmology = Albrecht von
842 Graefes Archiv fur klinische und experimentelle Ophthalmologie* 1996;234:440-444.
- 843 64. Lester M, Torre PG, Bricola G, Bagnis A, Calabria G. Retinal blood flow autoregulation
844 after dynamic exercise in healthy young subjects. *Ophthalmologica Journal international
845 d'ophtalmologie International journal of ophthalmology Zeitschrift fur Augenheilkunde*
846 2007;221:180-185.
- 847 65. Nemeth J, Knezy K, Tapaszto B, Kovacs R, Harkanyi Z. Different autoregulation response
848 to dynamic exercise in ophthalmic and central retinal arteries: a color Doppler study in healthy
849 subjects. *Graefe's archive for clinical and experimental ophthalmology = Albrecht von Graefes
850 Archiv fur klinische und experimentelle Ophthalmologie* 2002;240:835-840.
- 851 66. Morgan WH, Yu DY, Alder VA, et al. The correlation between cerebrospinal fluid
852 pressure and retrolaminar tissue pressure. *Investigative ophthalmology & visual science*
853 1998;39:1419-1428.
- 854 67. Ren R, Jonas JB, Tian G, et al. Cerebrospinal fluid pressure in glaucoma: a prospective

- study. *Ophthalmology* 2010;117:259-266.
68. Dorner GT, Polska E, Garhofer G, Zawinka C, Frank B, Schmetterer L. Calculation of the diameter of the central retinal artery from noninvasive measurements in humans. *Current eye research* 2002;25:341-345.
69. Dumskyj MJ, Eriksen JE, Dore CJ, Kohner EM. Autoregulation in the human retinal circulation: assessment using isometric exercise, laser Doppler velocimetry, and computer-assisted image analysis. *Microvascular research* 1996;51:378-392.
70. Feke GT, Pasquale LR. Retinal blood flow response to posture change in glaucoma patients compared with healthy subjects. *Ophthalmology* 2008;115:246-252.
71. Feke GT, Hazin R, Grosskreutz CL, Pasquale LR. Effect of brimonidine on retinal blood flow autoregulation in primary open-angle glaucoma. *Journal of ocular pharmacology and therapeutics : the official journal of the Association for Ocular Pharmacology and Therapeutics* 2011;27:347-352.
72. Grunwald JE, DuPont J, Riva CE. Retinal haemodynamics in patients with early diabetes mellitus. *The British journal of ophthalmology* 1996;80:327-331.
73. Strauss AL, Kedra AW. Experiences with a new procedure for the measurement of the ophthalmic artery pressure: ophthalmomanometry-Doppler. *Medical instrumentation* 1987;21:255-261.
74. Friedland AB. A mathematical model of transmural transport of oxygen to the retina. *Bulletin of mathematical biology* 1978;40:823-837.
75. *Clinical Methods: The History, Physical, and Laboratory Examinations*. 3rd ed: Boston: Butterworths; 1990.
76. Lakin WD, Stevens SA, Tranmer BI, Penar PL. A whole-body mathematical model for intracranial pressure dynamics. *Journal of mathematical biology* 2003;46:347-383.
77. Garcia JP, Jr., Garcia PT, Rosen RB. Retinal blood flow in the normal human eye using the canon laser blood flowmeter. *Ophthalmic research* 2002;34:295-299.
78. Riva CE, Grunwald JE, Sinclair SH, Petrig BL. Blood velocity and volumetric flow rate in human retinal vessels. *Investigative ophthalmology & visual science* 1985;26:1124-1132.
79. Yan D, McPheeters S, Johnson G, Utzinger U, Vande Geest JP. Microstructural differences in the human posterior sclera as a function of age and race. *Investigative ophthalmology & visual science* 2011;52:821-829.
80. Jonas JB. Ophthalmodynamometric assessment of the central retinal vein collapse pressure in eyes with retinal vein stasis or occlusion. *Graefe's archive for clinical and experimental ophthalmology = Albrecht von Graefes Archiv fur klinische und experimentelle Ophthalmologie* 2003;241:367-370.
81. Jonas JB. Ophthalmodynamometric measurement of orbital tissue pressure in thyroid-associated orbitopathy. *Acta ophthalmologica Scandinavica* 2004;82:239.
82. Sugiura Y, Okamoto F, Okamoto Y, Hasegawa Y, Hiraoka T, Oshika T. Ophthalmodynamometric pressure in eyes with proliferative diabetic retinopathy measured during pars plana vitrectomy. *American journal of ophthalmology* 2011;151:624-629 e621.
83. Jonas JB. Ophthalmodynamometric determination of the central retinal vessel collapse pressure correlated with systemic blood pressure. *The British journal of ophthalmology* 2004;88:501-504.
84. Glucksberg MR, Dunn R. Direct measurement of retinal microvascular pressures in the

- 899 live, anesthetized cat. *Microvascular research* 1993;45:158-165.
- 900 85. Attariwala R, Giebs CP, Glucksberg MR. The influence of elevated intraocular pressure
901 on vascular pressures in the cat retina. *Investigative ophthalmology & visual science*
902 1994;35:1019-1025.
- 903 86. Denardo SJ, Yamada EG, Hargrave VK, Yock PG. Effect of stenosis inlet geometry on
904 shear rates of blood flow in the upstream region. *American heart journal* 1993;125:350-356.
- 905 87. Woodman CR, Trott DW, Laughlin MH. Short-term increases in intraluminal pressure
906 reverse age-related decrements in endothelium-dependent dilation in soleus muscle feed
907 arteries. *J Appl Physiol (1985)* 2007;103:1172-1179.
- 908 88. Boltz A, Schmidl D, Werkmeister RM, et al. Regulation of optic nerve head blood flow
909 during combined changes in intraocular pressure and arterial blood pressure. *Journal of*
910 *cerebral blood flow and metabolism : official journal of the International Society of Cerebral*
911 *Blood Flow and Metabolism* 2013.
- 912 89. Chung HS, Harris A, Halter PJ, et al. Regional differences in retinal vascular reactivity.
913 *Investigative ophthalmology & visual science* 1999;40:2448-2453.
- 914 90. Verma S, Buchanan MR, Anderson TJ. Endothelial function testing as a biomarker of
915 vascular disease. *Circulation* 2003;108:2054-2059.
- 916 91. Pedley TJ, Brook BS, Seymour RS. Blood pressure and flow rate in the giraffe jugular
917 vein. *Philosophical transactions of the Royal Society of London Series B, Biological sciences*
918 1996;351:855-866.
- 919 92. Harris A, Jonescu-Cuypers, Kagemann L, Ciulla TA, Kriegstein GK. *Atlas of ocular blood*
920 *flow. Vascular anatomy, pathophysiology, and metabolism:* Elsevier; 2003.
- 921 93. Lee EJ, Kim TW, Weinreb RN. Variation of lamina cribrosa depth following
922 trabeculectomy. *Investigative ophthalmology & visual science* 2013;54:5392-5399.
- 923 94. Jonas JB, Holbach L. Central corneal thickness and thickness of the lamina cribrosa in
924 human eyes. *Investigative ophthalmology & visual science* 2005;46:1275-1279.
- 925 95. Ren R, Wang N, Li B, et al. Lamina cribrosa and peripapillary sclera histomorphometry in
926 normal and advanced glaucomatous Chinese eyes with various axial length. *Investigative*
927 *ophthalmology & visual science* 2009;50:2175-2184.
- 928 96. Fung YC. *Biomechanics: Circulation.* New York: Springer-Verlag; 1997.
- 929 97. Quarteroni A, Tuveri M, Veneziani A. Computational vascular fluid dynamics: problems,
930 models and methods. *Comput Visual Sci* 2000;2:163-197.
- 931 98. Armentano RL, Barra JG, Levenson J, Simon A, Pichel RH. Arterial wall mechanics in
932 conscious dogs. Assessment of viscous, inertial, and elastic moduli to characterize aortic wall
933 behavior. *Circulation research* 1995;76:468-478.
- 934 99. Fung YC. *Biomechanics: Mechanical Properties of Living Tissues.* 2nd ed. New York:
935 Springer-Verlag; 1993.
- 936 100. Deng X, Guidoin R. Arteries, veins and lymphatic vessels. *Handbook of biomaterial*
937 *properties:* Chapman & Hall; 1998:81-105.
- 938 101. Baleanu D, Ritt M, Harazny J, Heckmann J, Schmieder RE, Michelson G. Wall-to-lumen
939 ratio of retinal arterioles and arteriole-to-venule ratio of retinal vessels in patients with
940 cerebrovascular damage. *Investigative ophthalmology & visual science* 2009;50:4351-4359.
- 941 102. Wetterer E, Bauer RD, Pasch T. Arteriensystem. In: Bauereisen E, Bartels H,
942 Trendelenburg W, et al. (eds), *Physiologie des Kreislaufs* Berlin: Springer Verlag; 1971:1-66.

- 943 103. Jonas JB, Mardin CY, Schlotzer-Schrehardt U, Naumann GO. Morphometry of the human
944 lamina cribrosa surface. *Investigative ophthalmology & visual science* 1991;32:401-405.
- 945 104. Norman RE, Flanagan JG, Rausch SM, et al. Dimensions of the human sclera: Thickness
946 measurement and regional changes with axial length. *Experimental eye research*
947 2010;90:277-284.
- 948 105. Newson T, El-Sheikh A. Mathematical modeling of the biomechanics of the lamina
949 cribrosa under elevated intraocular pressures. *Journal of biomechanical engineering*
950 2006;128:496-504.
- 951 106. Woo SL, Kobayashi AS, Schlegel WA, Lawrence C. Nonlinear material properties of intact
952 cornea and sclera. *Experimental eye research* 1972;14:29-39.
- 953
- 954